Physics of the Earth and Planetary Interiors 381 (2026) 107618

Contents lists available at ScienceDirect

Physics of the Earth and Planetary Interiors

journal homepage: www.elsevier.com/locate/pepi

Effects of gyroremanence acquisition on anhysteretic remanence and the assessment of paleomagnetic stability: case of Pleistocene sediments offshore the western margin of Svalbard (IODP Exp-403)

Leonardo Sagnotti [a,*], Chiara Caricchi [a], Brendan Reilly [b], Lilla Spagnuolo [a], Renata G. Lucchi [c], Kristen St. John [d], Thomas A. Ronge [e], the IODP Exp 403 Scientists[1]

[a] Istituto Nazionale di Geofisica e Vulcanologia, Italy
[b] Lamont-Doherty Earth Observatory, Columbia University, USA
[c] Istituto Nazionale di Oceanografia e di Geofisica Sperimentale, Italy
[d] Department of Geology and Environmental Science, James Madison University, USA
[e] Texas A&M University, USA

ARTICLE INFO

Keywords:
Paleomagnetism
Rock magnetism
Arctic
Marine sediments
IODP Exp 403

ABSTRACT

Many Arctic sedimentary sequences exhibit complicated magnetizations, including long-lasting reversed intervals during expected normal polarity chronozones and frequent apparent geomagnetic excursions, although the underlying reasons vary. This study investigates the reliability of Pleistocene sediments as paleomagnetic recorders, focusing on u-channel samples from Site U1624 (IODP Expedition 403, Isfjorden drift), drilled in the Fram Strait between Greenland and Svalbard.

We used Arai plots constructed from stepwise anhysteretic remanent magnetization (ARM) acquisition and alternating field (AF) demagnetization up to 100 mT, to assess the reliability of paleomagnetic data. The paleomagnetic data show that the analyzed samples from Site U1624 exhibit substantial gyroremanent magnetization (GRM) during AF demagnetization of the natural remanent magnetization (NRM). This GRM acquisition significantly distorts the ARM-based Arai plots, rendering them unreliable for paleointensity estimation and detailed geomagnetic reconstructions within affected intervals. We identify correlations between GRM intensity and specific rock magnetic parameters, allowing us to (i) detect stratigraphic intervals dominated by single-domain ferrimagnetic minerals—such as clusters of diagenetic greigite grains—that induce GRM and bias ARM measurements, and (ii) evaluate which parameters serve as effective proxies for the concentration of GRM carriers.

In intervals where GRM acquisition is negligible, Arai plots based on ARM remain a robust tool for assessing the fidelity of the paleomagnetic signal and for constraining geomagnetic field variations. The proposed set of rock magnetic criteria therefore provides a framework to support the distinction between primary and diagenetically overprinted magnetizations in Arctic sedimentary records, improving their use for high-resolution geomagnetic and stratigraphic studies.

1. Introduction

In Pleistocene marine sedimentary cores from the Arctic, several reversed magnetizations have been identified during periods of expected normal polarity. These features persist longer than the typical 1–3 kyr duration of geomagnetic excursions (Nowaczyk et al., 1994; Nowaczyk and Baumann, 1992; Nowaczyk and Frederichs, 1999; Nowaczyk and Knies, 2000). Rock magnetic analyses indicate that often these signals represent apparent geomagnetic excursions and are the result of significant diagenetic alteration (e.g., Channell and Xuan, 2009; Xuan and Channell, 2010; Wiers et al., 2019, 2020), with the acquisition of a chemical remanent magnetization (CRM) carried by titanomaghemite, due to seafloor oxidation processes.

In contrast, reducing sediments sampled in the Fram Strait between

* Corresponding author.
E-mail address: leonardo.sagnotti@ingv.it (L. Sagnotti).
[1] https://iodp.tamu.edu/scienceops/precruise/easternfram/participants.html.

https://doi.org/10.1016/j.pepi.2026.107618
Received 7 July 2026; Received in revised form 14 October 2026; Accepted 18 October 2026
Available online 19 October 2026
0031-9201/© 2026 The Authors. Published by Elsevier B.V. This is an open access article under the CC BY-NC-ND license (http://creativecommons.org/licenses/by-nc-nd/4.0/).

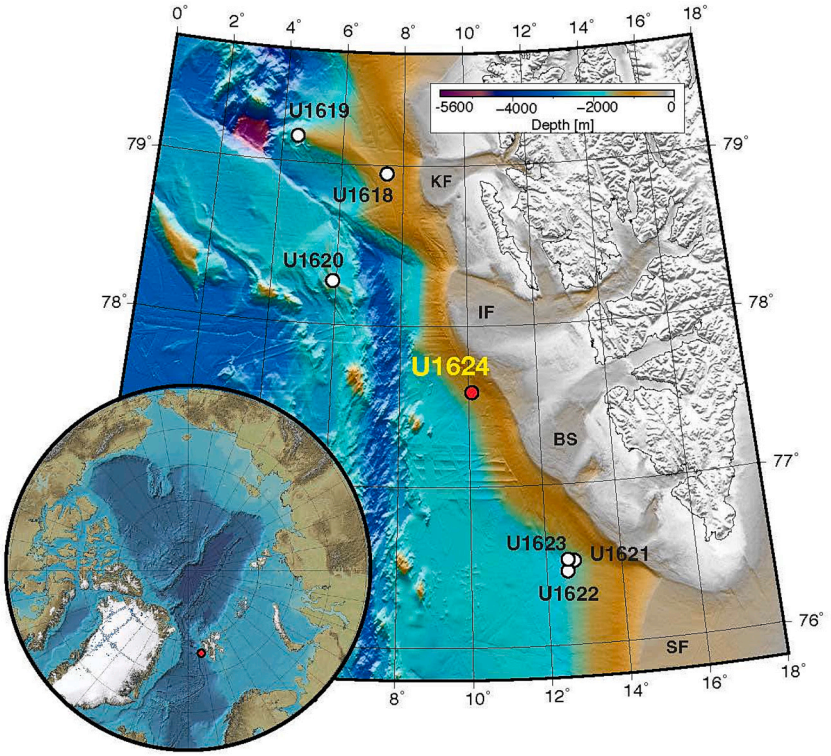

Fig. 1. Bathimetric map showing the location of Site U1624 on the Isfjorden sediment drift (IF) along the western margin of Svalbard. The map also shows the location of the other Sites of the IODP Expedition 403 (U1618-U1623) and the adjacent main glacial troughs: KF = Konsfjorden, BS = Bellsund, SF Storfjorden. Inset: IBCAO v3 map (Jakobsson et al., 2012) indicating the location of site U1624 in the Arctic area.

the North Atlantic and Arctic Oceans during IODP Exp. 403 often contained greigite as a common magnetic mineral (Lucchi et al., 2024, 2026; St. John et al., 2026). Early diagenetic greigite can acquire a remanence relatively close to deposition (Vasiliev et al., 2007, 2008). However, it is also well known that the occurrence of diagenetic greigite implies the acquisition of a CRM that may be significantly younger than deposition and may partially or fully overprint the primary detrital signal (e.g., Snowball, 1997; Roberts and Weaver, 2005; Sagnotti et al., 2005, 2010), resulting in "ghost polarities" or delayed magnetic signals. Greigite particles may also exhibit self-reversal properties that can mimic geomagnetic field reversal or excursions (Chang et al., 2023; Chen et al., 2026).

These examples demonstrate that diagenetic overprinting may obscure true geomagnetic signals in Arctic Ocean sediments. Such obscuration poses a major challenge to using paleomagnetic data from Arctic sedimentary sequences for stratigraphic correlation or age modelling. Developing rock magnetic techniques to help correctly interpret paleomagnetic signals from sedimentary sequences in the Arctic region would be an important step toward resolving this challenge.

The Arai plot is a key tool in paleomagnetism for assessing the reliability of paleointensity estimates of the Earth's magnetic field from the geological record (e.g. Nagata et al., 1963; Coe, 1967a; Paterson, 2011). A classic Arai plot (also called Thellier–Thellier or paleointensity plot) graphs the remaining natural remanent magnetization (NRM) against the acquired artificial remanent magnetization (e.g. anhysteretic remanent magnetization ARM or partial thermoremanent magnetization pTRM) at each demagnetization/locking step. The Arai plot can be also constructed using data from stepwise ARM acquisition and demagnetization cycles in progressively higher alternating fields (AF) (e.g., Tauxe et al., 1995; Yu et al., 2002). A linear segment on the data in the Arai plot corresponds to a stable magnetic component and its slope is proportional to the paleofield intensity. The presence of multi-domain particles, significant magnetic interactions, and/or variable magnetic mineralogy composition may produce curved Arai plots (sagging downward or "bowing") instead of straight lines, leading to under- or over-estimation of paleointensity if treated as linear (Coe, 1967b; Levi, 1977; Yu et al., 2002).

In this study we identify a set of rock magnetic experiments and parameters to assess the reliability of recovered Arctic sediments as paleomagnetic recorders of the fine details geomagnetic field variations. Our focus is on samples from Site U1624 of the IODP Expedition 403, in the Isfjorden sediment drift along the western continental margin of Svalbard (Lucchi et al., 2026) (Fig. 1). The analyzed samples show several intervals of significant gyroremanence (GRM) acquisition during stepwise AF demagnetization of their NRM and we discuss the effects of this GRM on the ARM data used to construct Arai plots. The results obtained in this study offer valuable insights into the impact of GRM on rock magnetic analyses derived from ARM data and show that significant GRM acquisition compromises the use of Arai plots for paleomagnetic reconstructions. Furthermore, we point out correlations between relevant rock magnetic parameters and provide criteria to detect stratigraphic intervals where diagenetic minerals, such as clusters of single-domain (SD) greigite particles, here identified by characteristic FORC diagrams, induce GRM and affect ARM analyses. We also discuss the efficiency of different rock magnetic parameters as proxies for the concentration of GRM carriers. These data may support the interpretation of the paleomagnetic features reported for marine sediments from the Fram Strait and Svalbard continental margin.

2. Materials and methods

Analyzed sediments were collected from Site U1624 during Expedition 403 of the International Ocean Discovery Program (IODP) (Lucchi et al., 2024, 2026). Site U1624 is located on the Isfjorden sediment drift, along the western continental margin of Svalbard, at a water depth of approximately 1320 m (Fig. 1).

The sediment drift lies between the Bellsund and Isfjorden trough

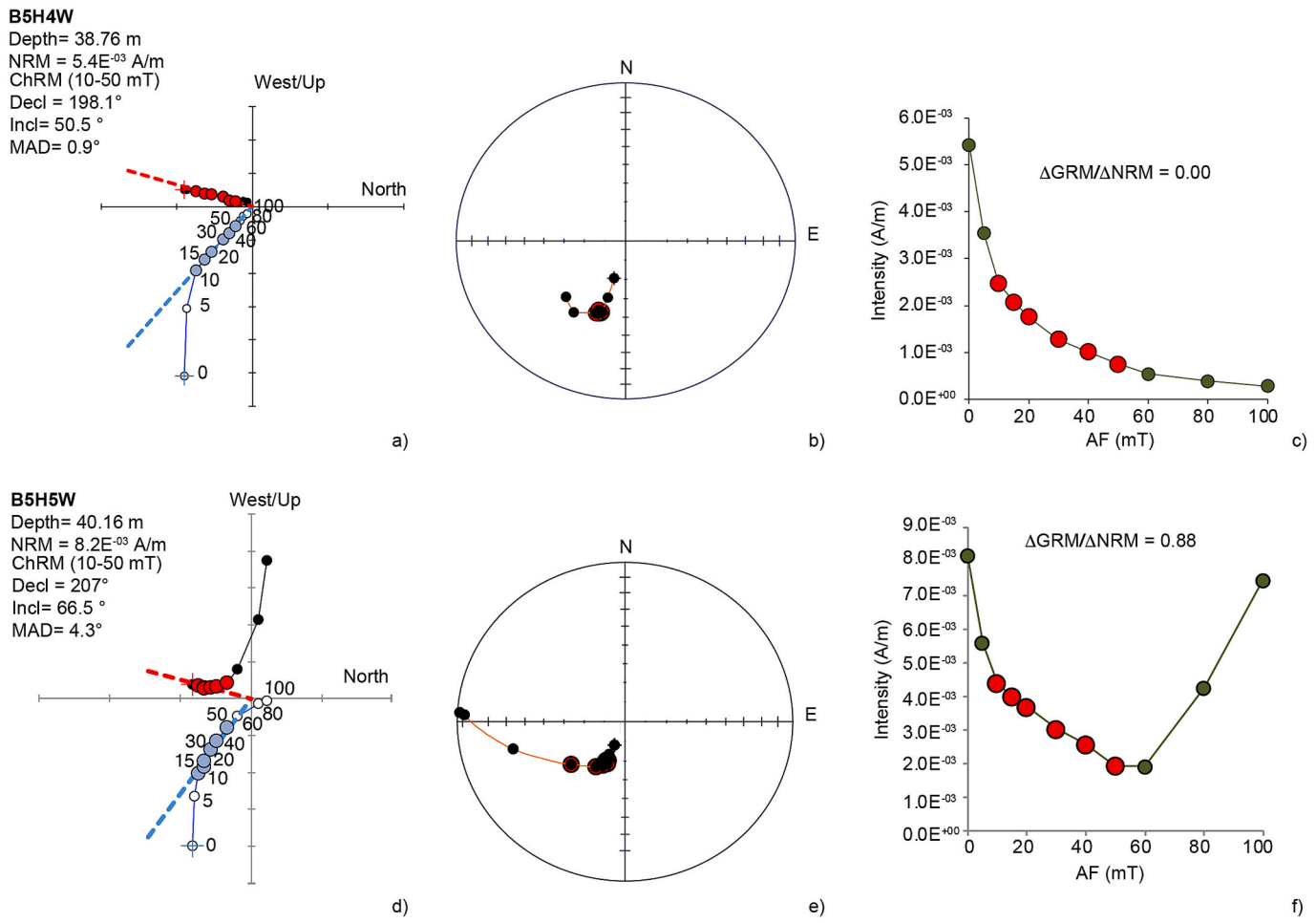

Fig. 2. Representative NRM demagnetization diagrams for measurements at position at 38.76 CCSF meter core composite depth below seafloor of u-channel U1624B-5H-4 W and 40.16 m CCSF of u-channel U1624B-5H-5 W, following stepwise AF demagnetization. a,d) orthogonal vector diagrams, b,e) stereographic (equal area) projections of unit vectors determined at each AF demagnetization step: black (open) symbols represent projection onto the lower (upper) hemisphere, c) NRM intensity versus peak AF. In a) and d) open and black circles represent projections onto vertical and horizontal planes, respectively. The data selected for ChRM determination are pointed out as coloured circles (red for horizontal plane, light blue for vertical plane). (For interpretation of the references to colour in this figure legend, the reader is referred to the web version of this article.)

mouth fans (TMFs), and it formed under the influence of the northward-flowing West Spitsbergen Current (WSC) transporting warm and saline North Atlantic Water to the Arctic Ocean through the Fram Strait (e.g., Schauer et al., 2004). Site U1624 consists of three drilled holes (U1624A, U1624B, and U1624C). Hole U1624A is very shallow, consisting of one 1.3 m long core, whereas Holes U1624B and U1624C were drilled to a maximum depth of 258 m below seafloor (mbsf), providing the complete sedimentary record of the site. These two deeper holes yielded substantial sediment recovery (over 200 m each) and their records were spliced to obtain a continuous and detailed stratigraphic sequence (composite sequence). The stratigraphic interval analyzed (0–128 m common stratigraphic composite depth, CCSF) contains the sediments forming Unit I composed by soft to firm dark gray, siliciclastic silty clay, with coarser intervals of reddish to dark reddish gray sandy mud and diamicton mainly occurring in the lower part of Unit I (Lucchi et al., 2026). This unit has been deposited during the Brunhes normal polarity Chron (Lucchi et al., 2026; St. John et al., 2026).

The working half sections of the composite sequence recovered at Site U1624 were sampled with u-channel plastic holders for paleomagnetic and rock magnetic measurements, carried out at the Istituto Nazionale di Geofisica e Vulcanologia in Rome (Italy). We collected 104 u-channels, spanning a stratigraphic interval of 120.82 m CCSF. For each u-channel we measured the low-field magnetic susceptibility (k) and the NRM at 1 cm spacing. The NRM was measured on a small-access (45-mm diameter) automated pass-through "2G Enterprises" DC 755 SRM and stepwise demagnetized in AF up to a peak field of 100 mT (steps: 0, 5, 10, 15, 20, 30, 40, 50, 60, 80, and 100 mT), translating the sample through a set of three perpendicular AF coils at a speed of 10 cm/s. The analysis of the demagnetization data was carried out by using the DAIE software (Sagnotti, 2013), applying principal component analysis on at least four consecutive demagnetization steps, to determine the characteristic remanent magnetization (ChRM) direction and the maximum angular deviation (MAD) for each measured interval.

Following the method developed by Fu et al. (2008), we computed the ΔGRM/ΔNRM ratio for all the measurements of the analyzed u-channels; ΔGRM represents the difference of the final intensity measured at the last AF step and the intensity minimum value (MV) during the whole AF treatment and ΔNRM represents the difference of initial intensity value and MV. The ΔGRM/ΔNRM ratio was computed by means of DAIE software (Sagnotti, 2013).

In this work we refer to 17 u-channels for which we analyzed stepwise acquisition and demagnetization of an ARM. In particular, we analyzed the working half of U1624B-5H (sections from 3 W to 6 W, 4 u-channels), U1624B-6H (sections from 2 W to 6 W, 5 u-channels), U1624C-5H (sections from 2 W to 6 W, 5 u-channels), U1624C-6H (sections from 4 W to 6 W, 3 u-channels). These u-channels span a stratigraphic interval from 36.5 to 56.3 m CCSF and were selected to include intervals characterized by swing from shallow to negative ChRM

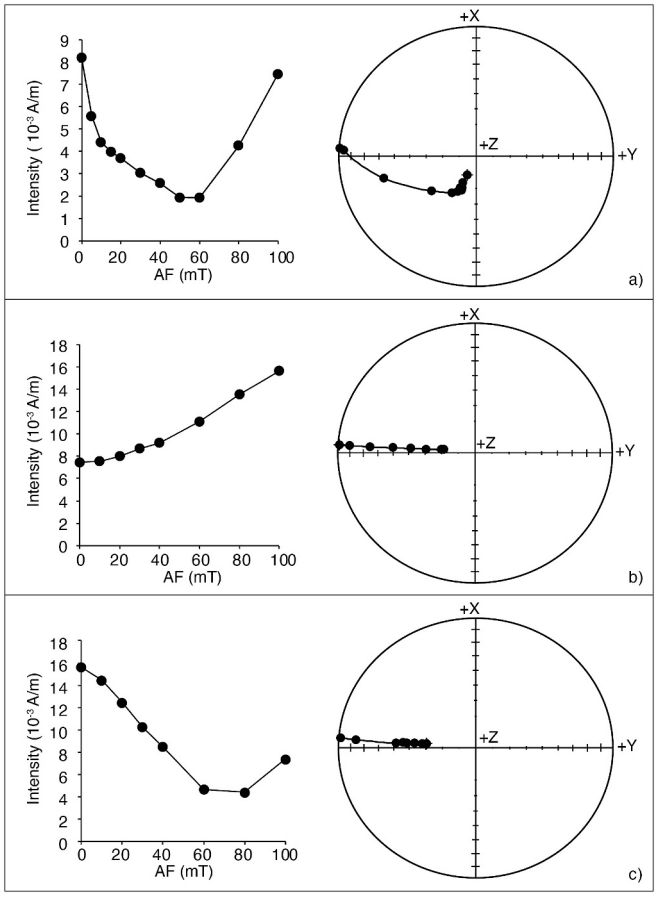

Fig. 3. Data for representative AF cycles of a stratigraphic position prone to significant GRM acquisition (U1624B-5H-5 W – 40.16 m CCSF, specimen's coordinates). a) NRM demagnetization cycle – ΔGRM/ΔNRM = 0.88; Remanence at the last AF step = 7.46×10^{-3} A/m. GRM acquisition develops at AF peak of 50 mT and higher, driving the remanence vector toward the horizontal plane; b) ARM acquisition cycle; initial remanence = 7.46×10^{-3} A/m. The ARM acquisition moves the remanence vector from horizontal toward the vertical axis; c) ARM demagnetization cycle – Remanence at the last AF step = 7.37×10^{-3} A/m. The ARM demagnetization and the new GRM acquisition drive the remanence vector from a relatively steep direction toward the horizontal plane.

inclinations. ARM was imparted by the simultaneous application of AF and an axial DC bias field of 50 μT (in AF steps of 10, 20, 30, 40, 60, 80 and 100 mT) and then demagnetized using the same AF steps, with the axial DC coil switched off.

The curvature of the Arai plot is determined by the best-fit circle to all the data (Paterson, 2011). To quantify the curvature, the parameter $\overrightarrow{k}$ was introduced, defined as the reciprocal of the radius (r) of the best-fit circle.

The analysis was performed at 1 cm stratigraphic intervals using a custom MATLAB routine based on the AraiCurvature.m function (Paterson, 2011). The software internally normalizes ARM intensities to a (0,1) range and applies robust least-squares circle-fitting algorithms (Taubin, 1991; Chernov and Lesort, 2005) to the data points.

The hysteresis properties of two samples collected in intervals of distinct ΔGRM/ΔNRM peaks were determined on powders hosted in pharmaceutical gel caps#4 with the vibrating sample magnetometer Lakeshore 8604 up to a field of 1.0 T at steps of 2.5 mT. First Order Reversal Curves (FORCs) (Roberts et al., 2000) were measured at steps of 3 mT, with 300 ms averaging time and maximum applied field being 1.0 T. FORC diagrams were processed and VARIFORC smoothed (Egli, 2013), smoothing factor of 3 and 4 respectively at the central and vertical ridges and of 7 at the background and drawn with the FORCINEL 3.06 Igor Pro routine (Harrison and Feinberg, 2008).

3. Results

The characteristic remanent magnetization (ChRM) of the analyzed sediments is typically isolated between 10 and 50 mT AF steps, with a steep inclination oscillating around the expected values for a geocentric axial dipole (GAD) field at high latitude (ca. 84° in this specific case). During the AF demagnetization of the NRM, several stratigraphic intervals acquired a gyroremanent magnetization, perpendicular to the axis of the last applied AF demagnetization coil (in our case the z-axis, that is the long axis of the u-channel sample), above 50–60 mT peak AF. At such fields, the NRM was reduced to about 10–15% of the initial value (Fig. 2). With acquisition of the GRM, the remanence directions show a distinct movement toward the xy plane of the u-channel reference system, so that at the last step of AF demagnetization (100 mT) the remanence of the stratigraphic intervals prone to GRM acquisition is almost sub-horizontal (Fig. 2e).

The acquisition of GRM is due to the irreversible flip of the moments of SD grains during AF demagnetization (Stephenson, 1980, 1993). Gyromagnetic effects can be helpful in rock magnetic studies and in particular the acquisition of GRM in marine and lacustrine sediments is widely used as a proxy for the occurrence of interacting SD greigite particles (e.g., Fu et al., 2008; Hu et al., 2002; Sagnotti and Winkler, 1999; Snowball, 1997; Stephenson and Snowball, 2001).

Greigite has been recognized as a common magnetic mineral in the sites sampled during IODP Exp 403 (Lucchi et al., 2024, 2026; St. John et al., 2026). Site U1624magnetic mineralogy mostly consists of detrital minerals, but the possible occurrence of a mixture of detrital magnetic minerals and authigenic greigite is anyway suggested by a bimodal distribution of the ARM_{30mT}/ARM parameter (see Fig. F11 of St. John et al., 2026).

In intervals prone to GRM acquisition, the GRM becomes evident above 50 mT during AF demagnetization of the NRM and increases exponentially with the peak field (Fig. 3a). This GRM is perpendicular to the last applied AF coil axis (the z-axis in specimen coordinates, which is equal to the vertical direction in the core's geographic coordinates), causing the remanence vector to deflect from the steep NRM direction toward the horizontal plane (Fig. 3a). In the following ARM acquisition cycle, the initial remanence does not begin from a fully demagnetized state; instead, it equals the GRM acquired at the end of the NRM demagnetization cycle. During ARM acquisition, the remanence vector shifts from the x-y plane toward the z-direction (Fig. 3b). However, at the end of the cycle, the vector remains significantly offset from the z-axis, along which the ARM was imparted by the axial DC coil. This suggests that the GRM interacts with the ARM, preventing full alignment with the z-axis. During subsequent AF demagnetization of the ARM, the composite remanence (ARM + GRM) demagnetizes with minimal directional change up to 60 mT. Beyond this point, the intensity rises again and the remanence vector is markedly displaced toward the x-y plane (Fig. 3c).

In intervals with no GRM acquisition, the remanence at the end of the NRM demagnetization cycle – which marks the start of stepwise ARM acquisition - is virtually negligible, as is the remanence remaining after ARM demagnetization. The imparted ARM then largely demagnetized over the same AF interval in which it was produced. As a result, the acquisition and demagnetization data follow the partial ARM reciprocity law (Yu et al., 2002): ARM blocking and unblocking are equivalent processes, yielding nearly linear Arai plots (Fig. 4a-d).

In contrast, intervals with significant GRM acquisition show a clear bias in the initial ARM state, with non-negligible starting remanence. ARM acquisition and demagnetization curves differ markedly, due to concurrent orthogonal GRM acquisition at high AF steps, which results in a pronounced curvature of the Arai plots (Fig. 4e-h).

During the initial steps of AF demagnetization, the NRM displays a

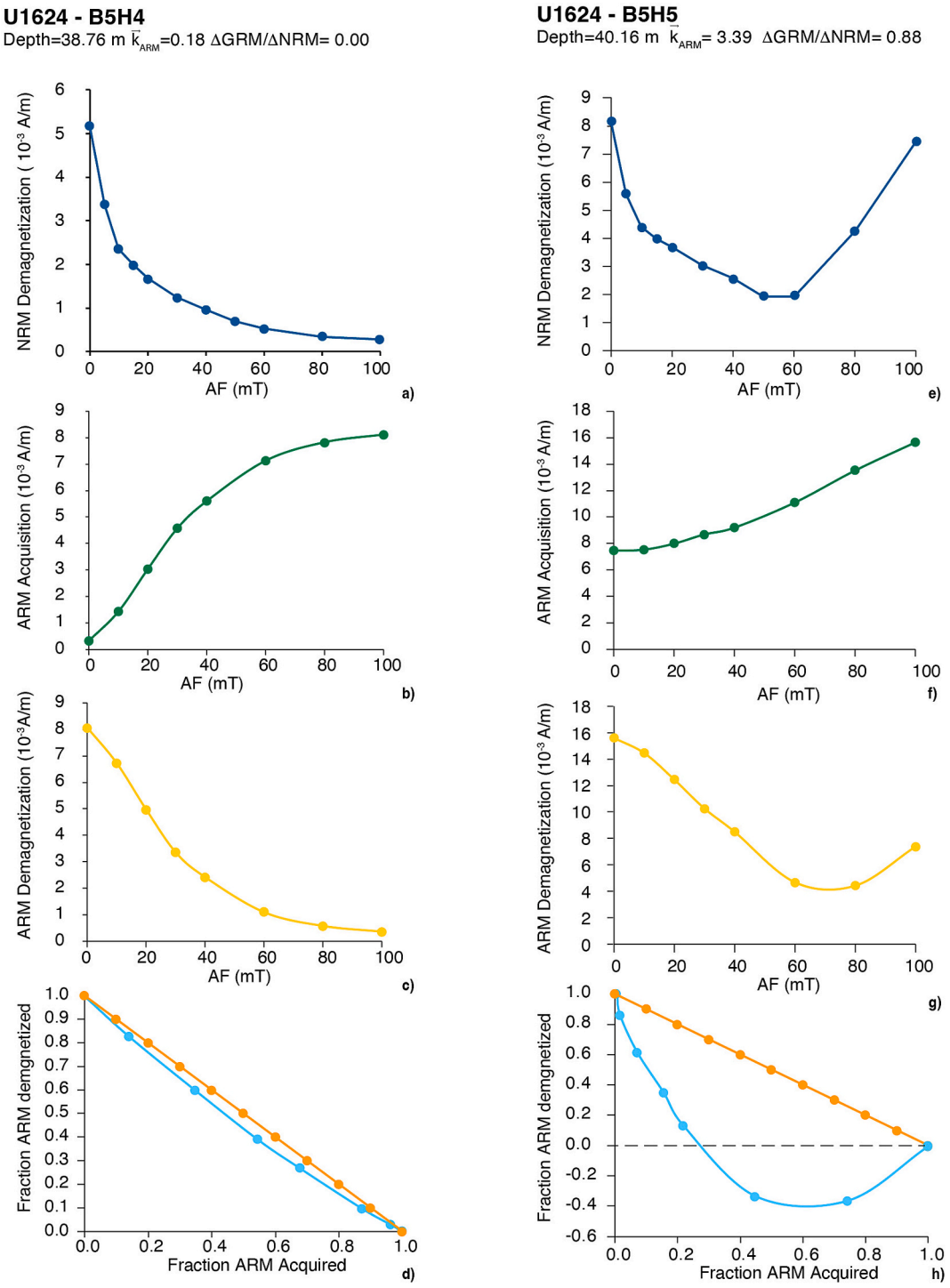

Fig. 4. NRM demagnetization (a, e), ARM acquisition (b, f), demagnetization (c, g) and Arai (d, h) plots for measurements at 38.76 m CCSF depth for u-channel U1624B-5H-4 W and at 40.16 m CCSF depth for u-channel U1624B-5H-5 W, following stepwise AF treatments. In the Arai plots the experimental data are indicated by the light blue curves and symbols and are compared with the theoretical data for a perfect reciprocity of ARM acquisition and demagnetization (orange line and symbols). (For interpretation of the references to colour in this figure legend, the reader is referred to the web version of this article.)

sharper intensity drop than the ARM (Fig. 4, plots a, c, e, g). This behavior is attributed to the removal of a low-coercivity viscous overprint, likely acquired during drilling operations (Acton et al., 2002; Richter et al., 2007); this overprint affects the NRM but not the laboratory-imparted ARM. At higher AF peaks (starting at 60 mT), the acquisition of a GRM impacts both the NRM and ARM (Fig. 4, plots e, g). However, the relative increase in GRM compared to the initial remanence intensity is more pronounced in the NRM than in the ARM. This difference likely stems from the higher initial intensity of the ARM compared to the NRM, since laboratory induction of ARM is far more efficient than natural sedimentary processes at aligning the magnetic moments of ferrimagnetic grains.

The ΔGRM/ΔNRM data obtained in this study reveal low or negligible GRM acquisition in several stratigraphic intervals: ~61% of the investigated sections have values <0.1, and ~ 17% have values <0.01. In contrast, GRM acquisition is significant in other intervals, where

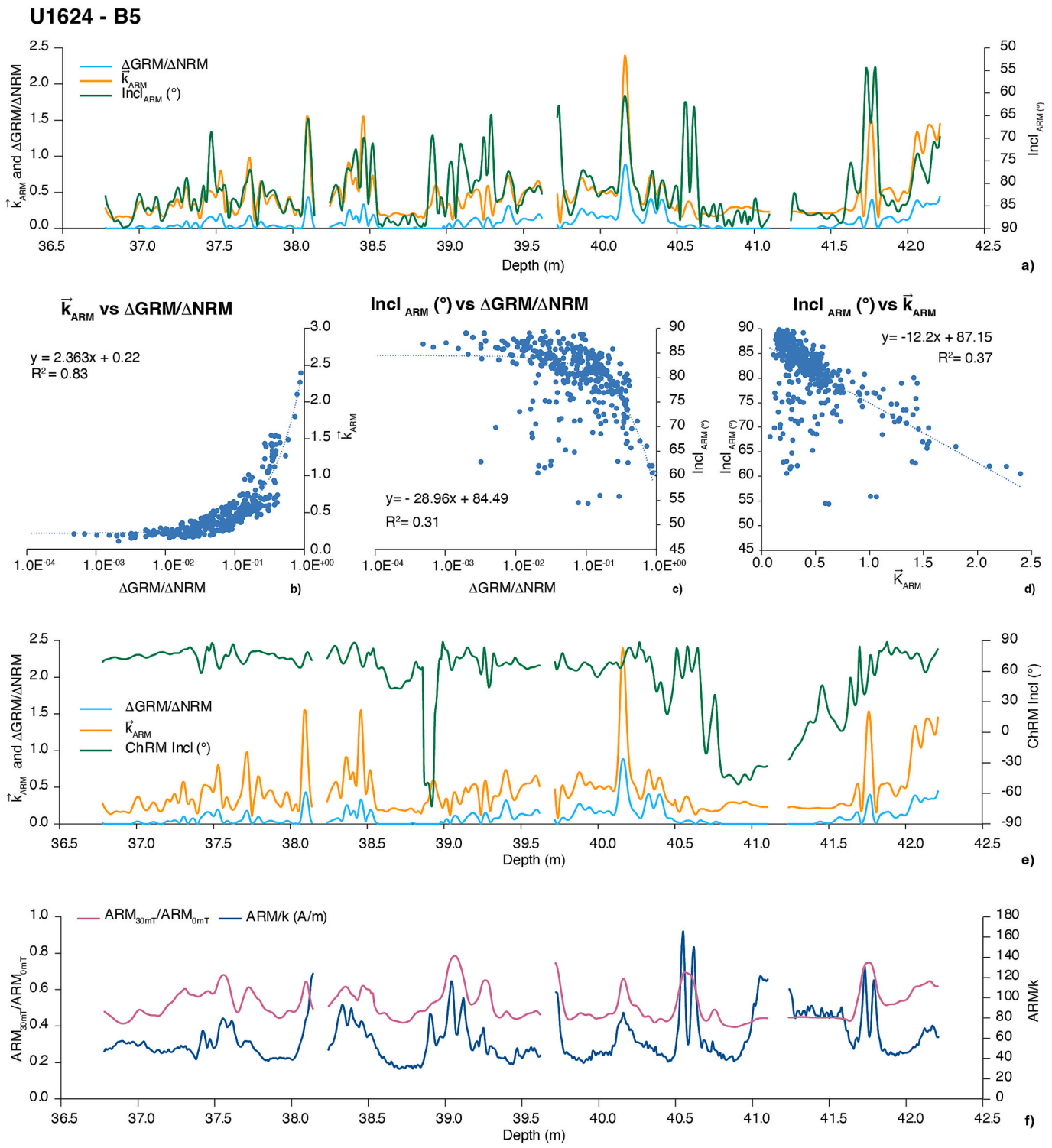

Fig. 5. Data obtained from the stratigraphic interval of U1624B-5H (4 u-channels spanning an interval from 36.78 to 42.21 m CCSF). a) Stratigraphic trends of the ΔGRM/ΔNRM ratio, the $\vec{k}_{ARM}$ parameter and the inclination of the ARM acquired at the highest AF step (100 mT); b), c) and d) scatter plots and parameters of linear correlation of the 3 couples of parameters shown in a). Note that in b) and c) the raw ΔGRM/ΔNRM data were plotted on a logarithmic scale. e) Stratigraphic trends of the ΔGRM/ΔNRM ratio, the $\vec{k}_{ARM}$ parameter and the inclination of the ChRM. f) Stratigraphic trend of the ARM_{30mT}/ARM_{0mT} and ARM/k parameters.

values typically range from 0.1 to 0.5 (overall span: 0–1.9) (Figs. 5 and 6).

The collected data indicate that the curvature of the Arai plot (represented by the $\vec{k}_{ARM}$ parameter) is correlated with the acquisition of a GRM at high AF peak (represented by the ΔGRM/ΔNRM ratio and by the shallowing of the ARM acquired at the last AF step). In Figs. 5 and 6 we show the main rock magnetic and paleomagnetic data for the stratigraphic intervals spanned by the U1624B-5H (sections from 3 W to 6 W, 4 u-channels) and U1624C-6H (sections from 4 W to 6 W, 3 u-channels), respectively. The correlation is higher for the $\vec{k}_{ARM}$ and ΔGRM/ΔNRM

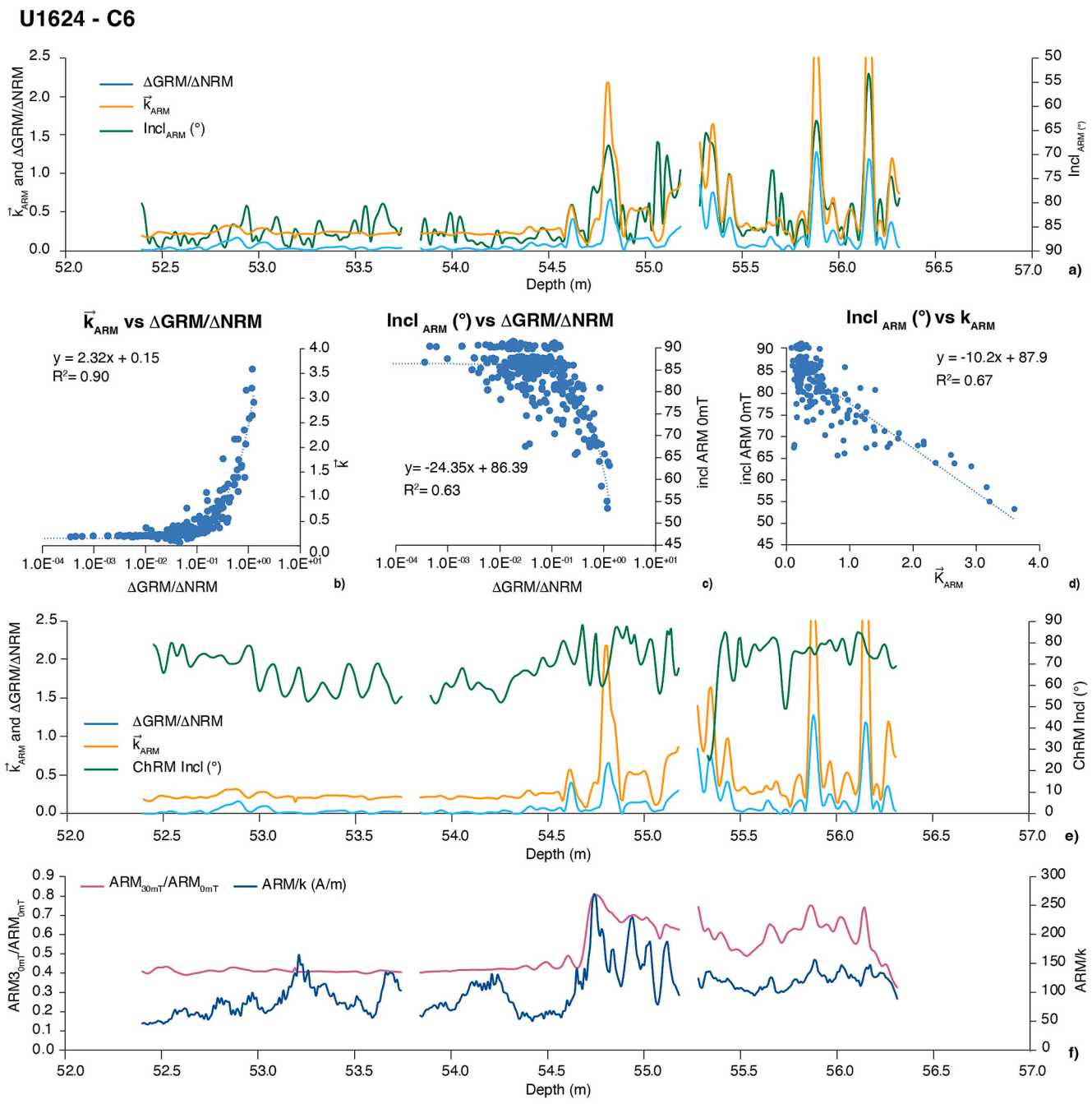

Fig. 6. Data obtained from the stratigraphic interval of U1624C-6H (3 u-channels spanning an interval from 52.40 to 56.31 m CCSF). a) Stratigraphic trends of the ΔGRM/ΔNRM ratio, the $\vec{k}_{ARM}$ parameter and the inclination of the ARM acquired at the highest AF step (100 mT); b), c) and d) scatter plots and parameters of linear correlation of the 3 couples of parameters shown in a). Note that in b) and c) the raw ΔGRM/ΔNRM data were plotted on a logarithmic scale. e) Stratigraphic trends of the ΔGRM/ΔNRM ratio, the $\vec{k}_{ARM}$ parameter and the inclination of the ChRM. f) Stratigraphic trend of the ARM_{30mT}/ARM_{0mT} and ARM/k parameters.

parameters (with R^2 value higher than 0.8) and the effects of the GRM acquisition are particularly evident for ΔGRM/ΔNRM values higher than 0.1 (Fig. 5b and Fig. 6b). The occurrence of evident swings to low or even reserve ChRM inclination values in some cases correspond to intervals with no GRM acquisition and almost linear Arai plots (e.g., Fig. 5e). A swing to low ChRM value observed at ca. 55.40 m composite depth (CCSF) at Site U1624 corresponds to a peak of GRM acquisition (Fig. 6e), but it occurs also at a u-channel break and we cannot exclude that it may also be due to disturbance during sampling and/or edge effects. Several other peaks of GRM acquisition and related curvature of the Arai plot do not correspond to anomalous ChRM inclination values.

The stratigraphic trends of ARM/k (a magnetic grain-size proxy) and the ARM_{30mT}/ARM_{0mT} ratios often match closely (Figs. 5f, 6f). The ARM_{30mT}/ARM_{0mT} ratio, which also depends on grain size, was previously used by Lucchi et al. (2024, 2026) as a proxy for greigite occurrence. A notable exception to the correlation occurs in the 41–41.7 CCSF interval of hole U1624B-5-H and the upper interval (52.5–54.5 CCSF) of hole U1624C-6-H, where the ARM_{30mT}/ARM_{0mT} trend remains virtually flat (Figs. 5f, 6f). The main peaks in the stratigraphic trends of the above mentioned grain-size dependent ratios occasionally coincide with peaks in GRM acquisition (e.g., at 38.1, 40.2, and 41.7 CCSF in core U1624B-5-H; Fig. 5), while in other instances they do not (e.g., at 39 and 40.5 CCSF in core U1624B-5-H; Fig. 5). This discrepancy suggests that the ΔGRM/ΔNRM parameter does not depend strictly on magnetic grain size.

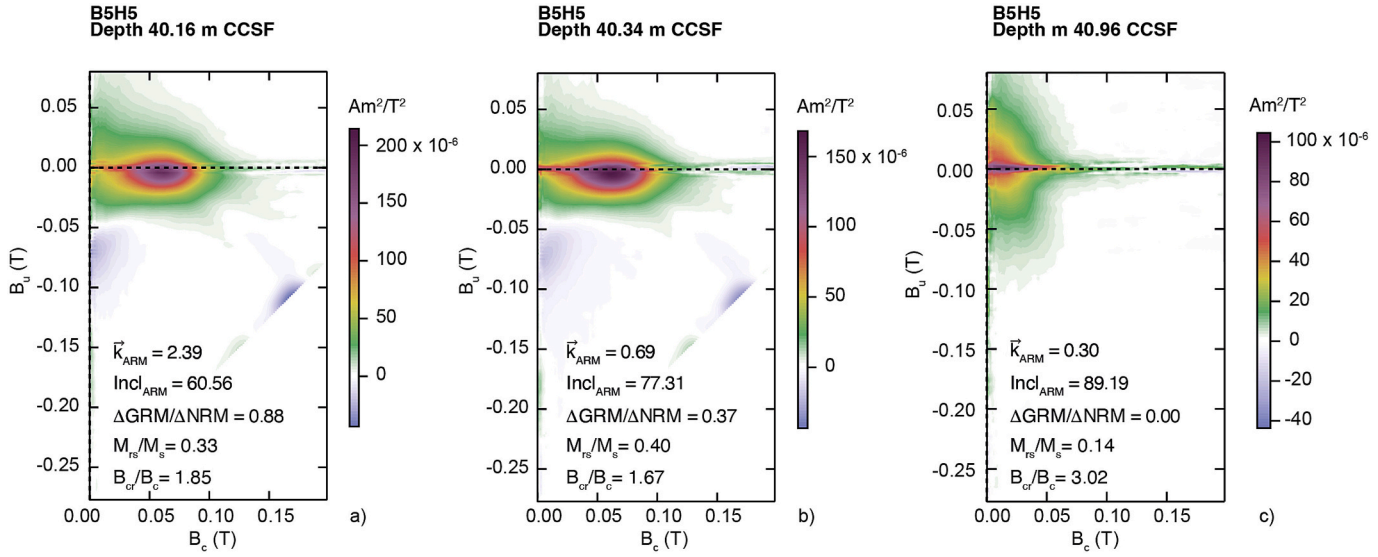

Fig. 7. FORC diagrams for selected samples from GRM acquisition peaks (a, b) and GRM-free (c) intervals. We used a smoothing factor of 3 and 4 respectively at the central and vertical ridges and of 7 at the background. The hysteresis ratios M_{rs}/M_s and B_{cr}/B_c are also indicated (M_{rs}: saturation remanent magnetization; M_s: saturation magnetization; B_{cr}: coercivity of remanence; B_c: coercivity).

Instead, it more likely reflects variations in magnetic mineralogy, signaling the presence and abundance of GRM-prone ferrimagnetic minerals.

The hysteresis properties and FORC diagrams of samples selected from distinct ΔGRM/ΔNRM peaks are typical for aggregates of prevailing SD greigite grains (Ding et al., 2024; Kars et al., 2021; Roberts et al., 2006; Sagnotti et al., 2010; Vasiliev et al., 2007). The FORC distribution displays closed, concentric contours centered around a high coercivity peak B_c between 50 mT and 80 mT (Fig. 7). Strong inter-grain magnetostatic interactions cause the concentric peak to spread vertically along the interaction field axis B_u. A distinct shift toward the origin of the primary SD peak indicates thermal relaxation typical of ultrafine superparamagnetic (SP) particles. The spread of contour lines outwards toward the B_u axis indicates an additional minor contribution of multi-domain (MD) grains. Conversely, the FORC diagram of a sample collected in a GRM-free interval shows features typical for pseudo-single domain (PSD) grains, with a distinctive closed-contour peak reminiscent of SD behavior, but with a broader distribution and more spread out along the horizontal coercivity axis (B_c); the central peak moves closer to the vertical interaction-field B_u axis, and the contours begin to diverge or intersect the B_u axis rather than remaining fully closed.

4. Discussion

In the analyzed sediments, a ChRM can be reliably isolated between 10 and 40–50 mT, before a GRM is eventually acquired at AF demagnetization steps of 60 mT or higher. At the last AF step considered for ChRM determination the NRM intensity drops to 10–15% of its initial value. GRM acquisition is absent in some stratigraphic intervals but prominent in others, where it forms peaks with end-of-cycle remanence values nearly matching the initial NRM intensity.

The FORC diagrams indicate that the magnetic carrier of the GRM is greigite occurring in aggregates of prevailing interacting SD grains and a mixture of subordinate SP and MD grains. In GRM-free intervals the paleomagnetic and rock magnetic properties indicate that the dominant remanence carrier is a low-coercivity magnetic mineral, mostly in a PSD state, that we link to detrital magnetite.

GRM induces pronounced curvature in Arai plots derived from ARM acquisition and demagnetization data. This effect becomes significant when GRM reaches a few percent of the NRM intensity lost during the AF stepwise demagnetization (starting from a ΔGRM/ΔNRM value of the order of 10^{-2}). The ΔGRM/ΔNRM ratio correlates linearly with the $\vec{k}_{ARM}$ parameter. The GRM vector, being perpendicular to the DC bias field axis during ARM acquisition, deflects ARM inclination from its theoretical 90° value in specimen coordinates. Consequently, Arai plot curvature also correlates linearly with ARM inclination, though this link is weaker than the ΔGRM/ΔNRM vs $\vec{k}_{ARM}$ relationship.

Unlike $\vec{k}_{ARM}$, which requires two additional AF cycles (for stepwise ARM acquisition and demagnetization), the ΔGRM/ΔNRM ratio can be measured directly from the NRM AF demagnetization curve. Thus, in intervals with significant GRM acquisition during NRM demagnetization the use of the Arai plot to assess SD vs. MD behavior – and evaluate paleomagnetic data reliability for paleosecular variation or paleointensity studies - is compromised.

However, the ΔGRM/ΔNRM parameter is ideal for single-component NRMs. Conversely, multicomponent or low-intensity NRMs introduce systematic offsets, hindering stratigraphic correlation and interpretation of GRM-prone carrier concentrations. In these scenarios, the use of the ARM inclination provides a reliable alternative. Like $\vec{k}_{ARM}$, it quantifies the horizontal GRM versus vertical ARM component. Because ARM inclination involves fewer measurement steps, it serves as a rapid estimate for GRM-bearing particle concentrations.

The identification of GRM-prone intervals serves as a proxy for the presence of diagenetic, SD greigite nodules. Because greigite can compromise the reliability of paleomagnetic records, its presence necessitates caution when interpreting fine-scale variations in the past geomagnetic field. However, we find no clear evidence of systematic differences in ChRM directional variability between GRM-prone and GRM-free intervals. While this lack of variance suggests that GRM-prone intervals may not suffer from a systematic directional bias, the precise timing of greigite nucleation, growth, and subsequent CRM acquisition relative to the depositional age of the hosting sediments remains largely unknown.

5. Conclusion

The acquisition of a GRM during AF stepwise demagnetization affects the use of the Arai plot based on progressive ARM acquisition and demagnetization to assess the reliability of paleomagnetic data. The curvature of the Arai plot is proportional to the acquisition of a GRM. The acquisition of a GRM during ARM acquisition produces also a

measurable deviation of the ARM direction from the axis of the applied DC field, which is vertical in the specimen coordinate system in our study case. This deviation, along with the ΔGRM/ΔNRM ratio, provides simple parameters to characterize and quantify a sample's tendency to acquire a GRM and a useful proxy for identifying clusters of SD greigite grains in sediments. The benefit of these approaches is that they are less dependent on the complicating properties of the NRM and thus offer another dimension to track the contribution of GRM carriers (such as clusters of SD greigite particles, here identified by characteristic FORC diagrams) that can be directly compared between different stratigraphic intervals.

In stratigraphic intervals lacking GRM acquisition, the Arai plot can safely be used to verify the reliability of paleomagnetic data. In our case study, intervals showing swings to low and/or reverse ChRM inclinations – with no GRM effects and a substantial reciprocity of partial ARM acquisition and demagnetization, resulting in nearly linear Arai plots - may possibly reflect true geomagnetic field excursions during the Brunhes Chron.

CRediT authorship contribution statement

Leonardo Sagnotti: Writing – review & editing, Writing – original draft, Visualization, Validation, Supervision, Methodology, Investigation, Formal analysis, Data curation, Conceptualization. **Chiara Caricchi:** Writing – review & editing, Writing – original draft, Validation, Methodology, Investigation, Formal analysis, Data curation, Conceptualization. **Brendan Reilly:** Writing – review & editing, Writing – original draft, Methodology, Investigation, Formal analysis, Data curation, Conceptualization. **Lilla Spagnuolo:** Writing – review & editing, Investigation, Data curation. **Renata G. Lucchi:** Writing – review & editing, Writing – original draft, Validation, Supervision, Investigation, Funding acquisition, Data curation. **Kristen St. John:** Writing – review & editing, Writing – original draft, Validation, Supervision. **Thomas A. Ronge:** Writing – review & editing, Writing – original draft, Validation.

Declaration of competing interest

The authors declare that they have no known competing financial interests or personal relationships that could have appeared to influence the work reported in this paper.

Acknowledgements

Special thanks go to the International Ocean Discovery Program Expedition 403 (Exp-403) project proponents, technicians, and crew. Funding for Exp-403 and the JOIDES Resolution Science Operator (JRSO) was provided via the National Science Foundation (NSF) award OCE1326927. We acknowledge research funding from MUR provided through ECORD-IODP Italia to CC and RGL. MAB acknowledges the project PID2021-126495NB-C33 funded by the Spanish Ministry of Science, Innovation and Universities. BTR received support from the US Science Support Program (USSSP), supported by the NSF award OCE1450528. This manuscript is a contribution to the project PRA2023_1 – AWARE, funded by the Arctic Research Program of Italy (PRA). We thank two anonymous Reviewers for their constructive comments and suggestions.

Data availability

Data will be made available on request.

References

Acton, G.D., Okada, M., Clement, B., Lund, S., Williams, T., 2002. Paleomagnetic overprints in ocean sediment cores and their relationship to shear deformation caused by piston coring. J. Geophys. Res. 107. https://doi.org/10.1029/2001JB000518.

Chang, L., Pei, Z., Xue, P., Wang, S., Wang, Z., Krijgsman, W., Dekkers, M.J., 2023. Self-reversed magnetization in sediments caused by greigite alteration. Geophys. Res. Lett. 50 (12), e2023GL103885. https://doi.org/10.1029/2023GL103885.

Channell, J.E.T., Xuan, C., 2009. Self-reversal and apparent magnetic excursions in arctic sediments. Earth Planet. Sci. Lett. 284, 124–131. https://doi.org/10.1016/j.epsl.2009.04.020.

Chen, S., Chang, L., Williams, W., 2026. Acquisition of self-reversed magnetization in greigite driven by antiparallel vortex-core coupling during low-temperature oxidation. Geophys. Res. Lett. 53, e2026GL121898. https://doi.org/10.1029/2026GL121898.

Chernov, N., Lesort, C., 2005. Least squares fitting of circles. J. Math. Imag. Vis. 23, 239–252. https://doi.org/10.1007/s10851-005-0482-8.

Coe, R.S., 1967a. Paleo-intensities of the earth's magnetic field determined from tertiary and quaternary rocks. J. Geophys. Res. 72, 3247–3262. https://doi.org/10.1029/JZ072i012p03247.

Coe, R.S., 1967b. The determination of paleointensities of the earth's magnetic field with special emphasis on mechanisms which could cause nonideal behavior in Thelliers' method. J. Geomagn. Geoelectr. 19, 157–179. https://doi.org/10.5636/jgg.19.157.

Ding, S., Dekkers, M.J., Li, M., Zhao, Q., Yan, Y., Zhu, Z., 2024. Rapid identification of greigite in lacustrine sediments using SIRM/χ and χARM: insights from the Cuo E core, Tibetan Plateau, China. Earth Space Sci. 11, e2024EA003508. https://doi.org/10.1029/2024EA003508.

Egli, R., 2013. VARIFORC: an optimized protocol for calculating non-regular first-order reversal curve (FORC) diagrams. Glob. Planet. Chang. 110, 302–320. https://doi.org/10.1016/j.gloplacha.2013.08.003.

Fu, Y., von Dobeneck, T., Franke, C., Heslop, D., Kasten, S., 2008. Rock magnetic identification and geochemical process models of greigite formation in quaternary marine sediments from the Gulf of Mexico (IODP Hole U1319A). Earth Planet. Sci. Lett. 275 (3), 233–245. https://doi.org/10.1016/j.epsl.2008.07.034.

Harrison, R.J., Feinberg, J.M., 2008. FORCinel: an improved algorithm for calculating first-order reversal curve distributions using locally weighted regression smoothing. Geochem. Geophys. Geosyst. 9 (5). https://doi.org/10.1029/2008GC001987.

Hu, S., Stephenson, A., Appel, E., 2002. A study of gyroremanent magnetisation (GRM) and rotational remanent magnetisation (RRM) carried by greigite from lake sediments. Geophys. J. Int. 151 (2), 469–474. https://doi.org/10.1046/j.1365-246X.2002.01793.x.

Jakobsson, M., Mayer, L.M., Coakley, B., Dowdeswell, J.A., Forbes, S., Fridman, B., Hodnesdal, H., Noormets, R., Pedersen, R., Rebesco, M., Schenke, H.W., Zarayskaya, Y., Accettella, D., Armstrong, A., Anderson, R.M., Bienhoff, P., Camerlenghi, A., Church, I., Edwards, M., Gardner, J.V., Hall, J.K., Hell, B., Hestvik, O., Kristoffersen, Y., Marcussen, C., Mohammad, R., Mosher, D., Nghiem, S. V., Pedrosa, M.T., Travaglini, P.G., Weatherall, P., 2012. The international bathymetric chart of the Arctic Ocean (IBCAO) version 3.0. Geophys. Res. Lett. 39, L12609. https://doi.org/10.1016/j.epsl.2008.07.034.

Kars, M., Greve, A., Zerbst, L., 2021. Authigenic greigite as an indicator of methane diffusion in gas hydrate-bearing sediments of the Hikurangi margin, New Zealand. Front. Earth Sci. 9, 603363. https://doi.org/10.3389/feart.2021.603363.

Levi, S., 1977. Effect of magnetite particle-size on paleointensity determinations of the geomagnetic-field. Phys. Earth Planet. Inter. 13, 245–259. https://doi.org/10.1016/0031-9201(77)90107-8.

Lucchi, R.G., St. John, K.E.K., Ronge, T.A., Barcena, M.A., De Schepper, S., Duxbury, L.C., Gebhardt, A.C., Gonzalez-Lanchas, A., Goss, G., Greco, N.M., Gruetzner, J., Haygood, L., Husum, K., Iizuka, M., Kapuge, A.K.I.U., Lam, A.R., Libman-Roshal, O., Liu, Y., Monito, L.R., Reilly, B.T., Rosenthal, Y., Sakai, Y., Sijinkumar, A.V., Suganuma, Y., Zhong, Y., 2026. Site U1624. In: Lucchi, R.G., St. John, K.E.K., Ronge, T.A., the Expedition 403 Scientists (Eds.), Eastern Fram Strait Paleo-Archive, Proceedings of the International Ocean Discovery Program, 403. International Ocean Discovery Program, College Station, TX. https://doi.org/10.14379/iodp.proc.403.107.2026.

Lucchi, R.G., St. John, K.E.K., Ronge, T.A., the Expedition 403 Scientists, 2024. Expedition 403 Preliminary Report: Eastern Fram Strait Paleo-Archive. International Ocean Discovery Program. https://doi.org/10.14379/iodp.pr.403.2024.

Nagata, T., Arai, Y., Momose, K., 1963. Secular variation of the geomagnetic total force during the last 5,000 years. J. Geophys. Res. 68, 5277–5281. https://doi.org/10.1029/j.2156-2202.1963.tb00005.x.

Nowaczyk, N.R., Baumann, M., 1992. Combined high-resolution magnetostratigraphy and nannofossil biostratigraphy for late Quaternary Arctic Ocean sediments. Deep-Sea Res. 39, 567–601. https://doi.org/10.1016/S0198-0149(06)80021-X.

Nowaczyk, N.R., Frederichs, T.W., 1999. Geomagnetic events and relative paleointensity variations during the last 300 ka as recorded in Kolbeinsey Ridge Sediments, Iceland Basin — indication for a strongly variable geomagnetic field. Int. J. Earth Sci. 88, 116–131. https://doi.org/10.1007/s005310050250.

Nowaczyk, N.R., Frederichs, T.W., Eisenhauer, A., Gard, G., 1994. Magnetostratigraphic data from late Quaternary sediments from the Yermak Plateau, Arctic Ocean: evidence for four geomagnetic polarity events within the last 170 Ka of the Brunhes Chron. Geophys. J. Int. 117, 453–471. https://doi.org/10.1111/j.1365-246X.1994.tb03944.x.

Nowaczyk, N.R., Knies, J., 2000. Magnetostratigraphic results from the eastern Arctic Ocean: AMS 14C ages and relative palaeointensity data of the Mono Lake and Laschamp geomagnetic reversal excursions. Geophys. J. Int. 140, 185–197. https://doi.org/10.1046/j.1365-246X.2000.00001.x.

Paterson, G.A., 2011. A simple test for the presence of multidomain behavior during paleointensity experiments. J. Geophys. Res. 116, B10104. https://doi.org/10.1029/2011JB008369.

Richter, C., Acton, G., Endris, C., Radsted, M., 2007. Handbook for shipboard paleomagnetists. In: ODP Tech. Note 34 available at https://www-odp.tamu.edu/publications/tnotes/tn34/tn34_.htm.

Roberts, A., Pike, C.R., Verosub, K.L., 2000. First-order reversal curve diagrams: a new tool for characterizing the magnetic properties of natural samples. J. Geophys. Res. 105, 28461–28475. https://doi.org/10.1029/2000JB900326.

Roberts, A.P., Liu, Q., Rowan, C.J., Chang, L., Carvallo, C., Torrent, J., Horng, C.-S., 2006. Characterization of hematite (α-Fe_2O_3), goethite (α-FeOOH), greigite (Fe_3S_4), and pyrrhotite (Fe_7S_8) using first-order reversal curve diagrams. J. Geophys. Res. 111, B12S35. https://doi.org/10.1029/2006JB004715.

Roberts, A.P., Weaver, R., 2005. Multiple mechanisms of remagnetization involving sedimentary greigite (Fe3 S4). Earth planet. Sci. Lett. 231, 263–277. https://doi.org/10.1016/j.epsl.2004.11.024.

Sagnotti, L., 2013. Demagnetization analysis in excel (DAIE) - an open source workbook in excel for viewing and analyzing demagnetization data from paleomagnetic discrete samples and u-channels. Ann. Geophys. 56 (1), D0114. https://doi.org/10.4401/ag-6282.

Sagnotti, L., Cascella, A., Ciaranfi, N., Macrì, P., Maiorano, P., Marino, M., Taddeucci, J., 2010. Rock magnetism and paleomagnetism of the Montalbano Jonico section (Italy): evidences for a late diagenetic growth of greigite and implications for magnetostratigraphy. Geophys. J. Int. 180, 1049–1066. https://doi.org/10.1111/j.1365-246X.2009.04480.x.

Sagnotti, L., Roberts, A.P., Weaver, R., Verosub, K.L., Florindo, F., Wilson, G.S., Pike, C. R., Clayton, T., 2005. Apparent high-frequency magnetic polarity reversals due to alternating remagnetization resulting from late diagenetic growth of greigite from siderite. Geophys. J. Int. 160, 89–100. https://doi.org/10.1111/j.1365-246X.2005.02485.x.

Sagnotti, L., Winkler, A., 1999. Rock magnetism and palaeomagnetism of greigite-bearing mudstones in the Italian peninsula. Earth Planet. Sci. Lett. 165, 67–80. https://doi.org/10.1016/S0012-821X(98)00248-9.

Schauer, U., Fahrbach, E., Osterhus, S., Rohardt, G., 2004. Arctic warming through the Fram Strait: oceanic heat transport from 3 years of measurements. J. Geophys. Res. 109, C06026. https://doi.org/10.1029/2003JC001823.

Snowball, I.F., 1997. Gyroremanent magnetization and the magnetic properties of greigite-bearing clays in southern Sweden. Geophys. J. Int. 129 (3), 624–636. https://doi.org/10.1111/j.1365-246X.1997.tb04498.x, 1413.

St. John, K.E.K., Lucchi, R.G., Ronge, T.A., Barcena, M.A., De Schepper, S., Duxbury, L.C., Gebhardt, A.C., Gonzalez-Lanchas, A., Goss, G., Greco, N.M., Gruetzner, J., Haygood, L., Husum, K., Iizuka, M., Kapuge, A.K.I.U., Lam, A.R., Libman-Roshal, O., Liu, Y., Monito, L.R., Reilly, B.T., Rosenthal, Y., Sakai, Y., Sijinkumar, A.V., Suganuma, Y., Zhong, Y., 2026. Expedition 403 summary. In: Lucchi, R.G., St. John, K.E.K., Ronge, T.A., the Expedition 403 Scientists (Eds.), Eastern Fram Strait Paleo-Archive. Proceedings of the International Ocean Discovery Program, 403. International Ocean Discovery Program, College Station, TX. https://doi.org/10.14379/iodp.proc.403.101.2026.

Stephenson, A., 1980. A gyroremanent magnetization in anisotropic magnetic minerals. Nature 84 (1980), 49–51. https://doi.org/10.1038/284049A0.

Stephenson, A., 1993. Three-axis static alternating field demagnetization of rocks and the identification of natural remanent magnetization, gyroremanent magnetization, and anisotropy. J. Geophys. Res. 98, 373–381. https://doi.org/10.1029/92JB01849.

Stephenson, A., Snowball, I.F., 2001. A large gyromagnetic effect in greigite. Geophys. J. Int. 145 (2), 570–575. https://doi.org/10.1046/j.0956-540x.2001.01434.x.

Taubin, G., 1991. Estimation of planar curves, surfaces, and nonplanar space curves defined by implicit equations with applications to edge and range image segmentation. IEEE Trans. Pattern Anal. Mach. Intell. 13, 1115–1138. https://doi.org/10.1109/34.103273.

Tauxe, L., Pick, T., Kok, Y.S., 1995. Relative paleointensity in sediments: a pseudo-Thellier approach. Geophys. Res. Lett. 22, 2885–2888. https://doi.org/10.1029/95GL03166.

Vasiliev, I., Dekkers, M.J., Krijgsman, W., Franke, C., Langereis, C.G., Mullender, T.A.T., 2007. Early diagenetic greigite as a recorder of the palaeomagnetic signal in Miocene—Pliocene sedimentary rocks of the Carpathian foredeep (Romania). Geophys. J. Int. 171 (2), 613–629. https://doi.org/10.1111/j.1365-246X.2007.03560.x.

Vasiliev, I., Franke, C., Meeldijk, J.D., Dekkers, M.J., Langereis, C.G., Krijgsman, W., 2008. Putative greigite magnetofossils from the Pliocene epoch. Nat. Geosci. 1, 782–786. https://doi.org/10.1038/ngeo335.

Wiers, S., Snowball, I., O'Regan, M., Almqvist, B., 2019. Late Pleistocene chronology of sediments from the Yermak Plateau and uncertainty in dating based on geomagnetic excursions. Geochem. Geophys. Geosyst. 20, 3289–3310. https://doi.org/10.1029/2018GC007920.

Wiers, S., Snowball, I., O'Regan, M., Pearce, C., Almqvist, B., 2020. The Arctic Ocean manganese cycle, an overlooked mechanism in the anomalous palaeomagnetic sedimentary record. Front. Earth Sci. 8, 75. https://doi.org/10.3389/feart.2020.00075.

Xuan, C., Channell, J.E.T., 2010. Origin of apparent magnetic excursions in deep-sea sediments from Mendeleev-Alpha Ridge, Arctic Ocean. Geochem. Geophys. Geosyst. 11, 1–17. https://doi.org/10.1029/2009gc002879.

Yu, Y., Dunlop, D.J., Özdemir, Ö., 2002. Partial anhysteretic remanent magnetization in magnetite, 2, reciprocity. J. Geophys. Res. 107 (B10), 2245. https://doi.org/10.1029/2001JB001269.